J Mol Model (2014) 20:2534
DOI 10.1007/s00894-014-2534-8

ORIGINAL PAPER

Role of size and shape selectivity in interaction between gold nanoclusters and imidazole: a theoretical study

Muthuramalingam Prakash · Gilberte Chambaud · M. Mogren Al-Mogren · Majdi Hochlaf

Received: 29 May 2014 / Accepted: 17 November 2014 / Published online: 9 December 2014

Abstract We present a theoretical study on the structure, stability, spectra and electronic properties of imidazole (*Im*) adsorbed on gold nanoclusters (Au_n, n=2, 4, 6, 8, 10, and 20). These computations were performed using various density functional theories with and without inclusion of Grimme's (D3) dispersion correction. For small clusters, we also carried out wavefunction-based ab initio (MP2 and SCS-MP2) computations for comparison. Vibrational, atoms in molecules (AIM) and natural bond orbital (NBO) analyses clearly reveal the occurrence of charge transfer (CT) through covalent (N1–Au) and noncovalent interactions that play important roles in the stability of the *Im*@Au_n complexes with anchor assisted H-bonds (C_α–H·Au). Therefore, gold clusters can act as H-bond acceptors with biomolecules for development of new materials and applications. Our study establishes also the ability and reliability of PBE0 and M05-2X functionals compared to B3LYP and PBE for an accurate description of covalent and noncovalent interactions between *Im* and gold clusters since they lead to close agreement with MP2. Finally, we show that the Au_8 cluster may be viewed as large enough to mimic the 3D gold surface.

Keywords Gold clusters · Bio-molecules · NBO · AIM · Ab Initio · TDDFT

Electronic supplementary material The online version of this article (doi:10.1007/s00894-014-2534-8) contains supplementary material, which is available to authorized users.

M. Prakash · G. Chambaud · M. Hochlaf (✉)
Laboratoire Modélisation et Simulation Multi Echelle, MSME UMR, Université Paris-Est, 8208 CNRS, 5 bd Descartes, 77454 Marne-la-Vallée, France
e-mail: hochlaf@univ-mlv.fr

M. M. Al-Mogren
Chemistry Department, Faculty of Science, King Saud University, PO Box 2455, Riyadh 11451, Kingdom of Saudi Arabia

Introduction

Gold bulk surfaces have relatively high inertness in any chemical environment. [1] Therefore, adsorption of molecules on such surfaces is difficult, whereas reactivity as well as adsorption capacity on Au_n clusters vary and depend strongly on clusters size, i.e., n. This may be connected to the possible different Au–Au coordination numbers in Au_n clusters. Particularly, inner gold Au–Au bonds are always shorter and stronger than the outer bonds [2–6]. Specifically, investigations into the interaction of biomolecules with gold nanoparticles (Au_n, n=1–20/40 called also nanoclusters) represent a very active research topic in biological, chemical and material sciences [7–23]. These features can play important roles in various fields of application of gold complexes, such as sensors, biosensors, drug-delivery, molecular electronic devices and energy materials [7, 8, 9].

Numerous experimental and theoretical studies have been performed on the complexes formed between various sizes of selected Au_n nanoparticles and biomolecules such as DNA bases, proteins, peptides and nitrogen-based bases for biochemical applications [10–23]. For instance, nitrogen based biomolecules such as guanine (G) [10, 11], cytosine (C) [12, 13], adenine (A) [14], thymine (T) [15], uracil (U) [16], histidine (HIS) [17], cysteamine [18] and DNA base pairs (AT and GC) [19–23], with gold clusters and surfaces have attracted widespread attention. For gold clusters binding with nucleic acid base pairs (GC@Au_n and AT@Au_n, where n=4 and 8), DFT-B3LYP calculations by Kumar et al. [14] revealed that neutral gold complexes are more stable than the corresponding anions. Using also B3LYP method, Leszczynski and co-workers [21] studied the interaction of purine base G, and the Watson-Crick GC base pair with gold nanoclusters. They reported vertical ionization energies, electron affinities and charge transfer characteristics for these complexes. These studies clearly revealed that A, G, and C

adsorb at Au electrodes whereas base unit T does not, which is in line with the experimental studies by Tao et al. [24] of nucleic acid bases in interaction with the Au (111) surface. Accordingly, strong binding of the N-atom on gold surface/nanoclusters requires an unprotonated nitrogen part of the aromatic ring.

Another important issue relative to the investigation of molecules–gold nanoclusters concerns the quantification with high accuracy of various types of covalent and noncovalent interactions that may take place during chemisorption and physisorption of molecules on gold surfaces. The strength and nature of the interactions between organic adsorbate and metal substrate can be probed experimentally through, for instance, temperature-programmed desorption (TPD) and microcalorimetry measurements [25, 26]. Alternatively, theoretical approaches can be used to predict the structure, stability, bonding, binding sites and properties of these nanomaterials. In 2006, Aikens and Schatz [27] pointed out a chemical surface-enhanced Raman scattering (SERS) enhancement for pyridine linked to Au_{20} cluster (i.e., pyridine@Au_{20}) using time dependent-density functional theory (TD-DFT) and SERS spectroscopy; however, the origins of such enhancement were not definitively established. In 2008, Iori et al. [17] treated the interaction between the HIS (*Im* model) side chain and the Au (111) surface using DFT-PBE. They established the existence of an unconventional H-bond (namely a C_α–H···Au bond) that is uncertain in DNA base pairs and a HIS model with Au (111) surface [17]. Moreover, they found that the unprotonated N1 atom of the *Im* moiety interacts directly with the top site of the fcc (111) hexagonal lattice [17]. In 2012, Cao and co-workers [28] found an unconventional N–H···Au H-bond in nucleobase–gold complexes through anion photoelectron spectroscopy and DFT calculations. Last year, experimental and theoretical reports on various phases of benzenediamine molecules with gold surface using X-ray resonant photoemission spectroscopy (RPES) revealed that ultrafast charge transfer (CT) across the metal–organic interface does not require solely covalent bonds but may occur also through noncovalent interactions [29].

Generally, gold interacts with N-based biomolecules through CT, van der Waals (vdWs), and hydrogen (H)-bonded interactions such as N–H···Au, C2–H···Au, and C5–H···Au types of interaction (see Fig. 1 for atom numbering). These unconventional types of H-bonds can be calculated by modern experimental and theoretical techniques [28]. Theoretically, quantification of CT through covalent and noncovalent interactions within organic-metal clusters can be evaluated from selection of a suitable functional. With this purpose in mind, Urban and co-workers characterized the type of metal–ligand interaction, bonding and CT properties of coinage metals and lone-pair ligands using different DFTs and CCSD (T) methods in connection with relativistic basis sets [30], and showed that the PBE0 functional is well suited to treating these kinds of complexes. At present, we use a set of exchange correlation density functionals (i.e., B3LYP, PBE, PBE0 and M05-2X) in connection with large basis sets to deduce the equilibrium structures, energetics, spectroscopy and chemical bond types (covalent, CT, vdWs) in *Im*@Au_n complexes, where n=2, 4, 6, 8, 10, and 20. We first check the capability of various DFT functionals for deriving reliable data for *Im*@Au_n through comparison to MP2 geometries and energetics for smaller *Im*@Au_n (n=2 and 4) complexes. We also considered dispersion effects via inclusion of Grimme's corrections. Based on the evaluation, we select PBE0 and M05-2X functionals for the treatment of larger sized clusters (n=6–20). Mainly, we show that *Im*@Au_n properties (both structural parameters and binding energies (BEs) converge to those of *Im* adsorbed on Au bulk for n ~8 and that *Im*@Au_n complexes are stabilized by a strong nitrogen–gold bond together with weak anchor assisted H-bond (AAHB) interactions. Finally, we discuss the possible applications of the present findings.

Computational details

Difficulties in studying organic-metal cluster complexes reside in: (1) a balanced description of metal–metal and metal–hetero atoms within the complexes, (2) the correct accounting for electron correlation and dispersion that plays a crucial role in their bonding and structure, (3) the accurate description of several types of interactions that are a priori in action (e.g., covalent bonding within *Im*, Au–Au bond and covalent and/or non-covalent Au–*Im* bondings). Our approach overcomes all these difficulties, leading to accurate predictions for *Im*@Au_n complexes.

For the description of H, C, N atoms, we used either 6–31+G** or aug-cc-pVTZ basis sets [31–33]. Gold atoms were described using the Los Alamos effective core potential (ECP) Lanl2DZ [34] and the associated 6-31+G**ULanl2DZ basis set (denoted hereafter as BS1) or aug-cc-pVTZULanl2DZ basis set (denoted as BS2).

For geometry optimizations, we used GAUSSIAN 09 [35]. We considered closed-shell configuration for *Im*@Au_n (n=2, 4, 6, 8, 10, and 20) complexes, which are taken in their ground singlet states. Following the investigations of Tao et al. [24], we looked for nanoclusters linking to the unprotonated nitrogen of *Im* since the other sites would lead to less stable isomers of *Im*@Au_n. The initial structures of these complexes were inspired from those of the corresponding isolated Au_n clusters as established elsewhere [36–39]. Most of them are detailed in a review by Häkkinen [5] and references therein. The *Im*@Au_n equilibrium geometries were then freely optimized using DFT-B3LYP, PBE, and PBE0 methods. In addition, we used the M05-2X functional. Recent reports on this kind of molecular systems proved that the M05-2X method is a priori well suited for

accurate description of vdWs and dispersion interactions [40–44]. Indeed, close agreement was noted between M05-2X results and those derived using CCSD(T)/CBS on hydride ion–water clusters [45]. All optimizations were performed with Opt=tight and Int=Ultrafine keywords of GAUSSIAN 09. For some complexes, additional SCF=QC or XQC keywords were used to force convergence. Further Møller-Plesset (MP2) [46] and spin-component scaled MP2 (SCS-MP2) [47] computations were carried out for *Im*@Au_2 and *Im*@Au_4 to benchmark suitable DFT methods for the treatment of the larger *Im*@Au_n complexes. These computations were performed using the MOLPRO (version 2012.1) package [48]. Recent reports on H-bonded and stacked dimers have clearly established that SCS-MP2 is well suited for stacking whereas MP2 describes H-bonded dimers well [49]. To address long-range interactions, such as H-bonding and vdWs, we performed additional computations where we used Grimme's latest version of empirical correction term (DFT-D3) [50–52]. These computations consist of single-point energy correction for geometries optimized using PBE0 and M05-2X methods.

To quantify the nature of intermolecular interactions of CT between *Im* and gold clusters and of the strength of AAHBs within *Im*@Au_n clusters, we calculated the vibrational frequencies of these clusters and performed atoms-in-molecules (AIM) analysis as implemented in the AIM 2000 package [53]. AIM is a useful tool to probe covalent and possible weakly bonded systems including vdWs complexes [54–59]. The wave function was generated from M05-2X/BS1 calculation using optimized geometry at the same level. In addition, we analyzed the CT properties between gold clusters and *Im* using an NBO [60] approach. NBO analysis was carried out at PBE0/BS1 level of theory. Details of the corresponding analysis and the full set of results are given in the electronic supplementary material (ESM).

Results and discussion

Figures 1, 2, 3, 4, 5 and 6 display the optimized structures of *Im*@Au_n (*n*=2, 4, 6, 8, 10, and 20). All represent equilibrium structures, all with positive frequencies. The main geometrical parameters computed at DFT-B3LYP, PBE, PBE0 and M05-2X are given, in connection with the BS1 basis set for comparison. The calculated binding energies (BEs) are listed in Tables 1 and 2. For the *Im* moiety adsorbed on Au_n clusters, similar equilibrium geometries were found. For Im@Au_n (*n*=2, 4), we present also those deduced using the larger BS2 basis set. Moreover, further computations at the MP2/BS1 and MP2/BS2 levels were also carried out for these two complexes. The respective MP2 and SCS-MP2 BEs are provided in Table 1.

Equilibrium geometries of Im@Au_n clusters and bonding

Im@Au₂

At all levels of theory, we found a planar Im@Au_2 stable complex (Fig. 1). This is due to the non-disturbing environment from the gold side (i.e., linear) with perfect orbital interaction between N1 and Au atoms (Fig. S1 in ESM). DFT Au-N1 equilibrium distances are 2.149 (2.117), 2.110 (2.077), 2.116 (2.0847) and 2.146 (2.124) Å and the Au–Au equilibrium distances are 2.568 (2.565), 2.550 (2.545), 2.541 (2.538) and 2.550 (2.546) Å, using the BS1 (BS2) basis set (Fig. 1). Therefore, BS2 leads to slightly shorter equilibrium distances (differences are less than 0.03 Å). MP2 predicts equilibrium distances within the same range as DFT methods. Earlier reports on G@Au_2 complex optimized at B3LYP/BS1 derived Au–N and Au–Au distances of 2.162 Å and 2.569 Å, respectively [10]. These results are in close agreement with ours at the same level of theory. For both G@Au_2 and Im@Au_2 complexes, the Au–Au distance is slightly longer

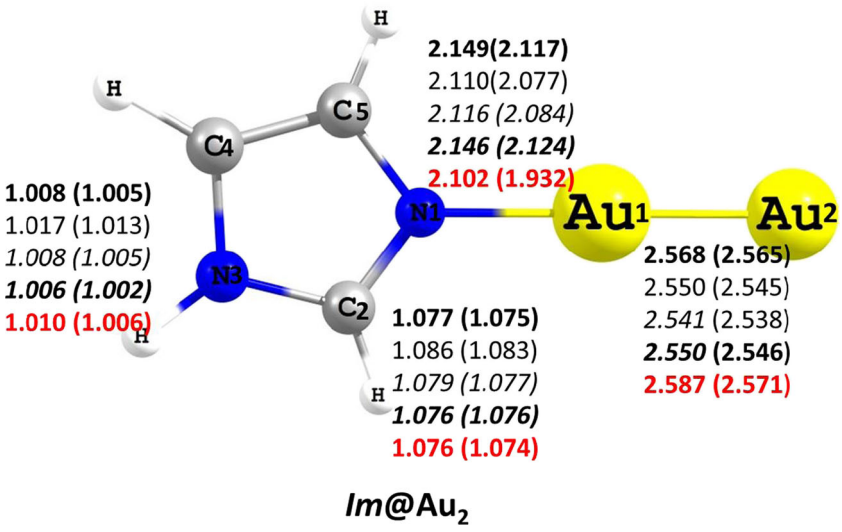

Fig. 1 Optimized geometries of *Im*@Au_2 at B3LYP (*bold*), PBE (*normal*), PBE0 (*Italic*) and M05-2X (*bold / italic*) methods using BS1 basis set. Parenthesed distances are computed using BS2. Geometries at MP2 level are presented in *red*. Distances are in Ångstroms

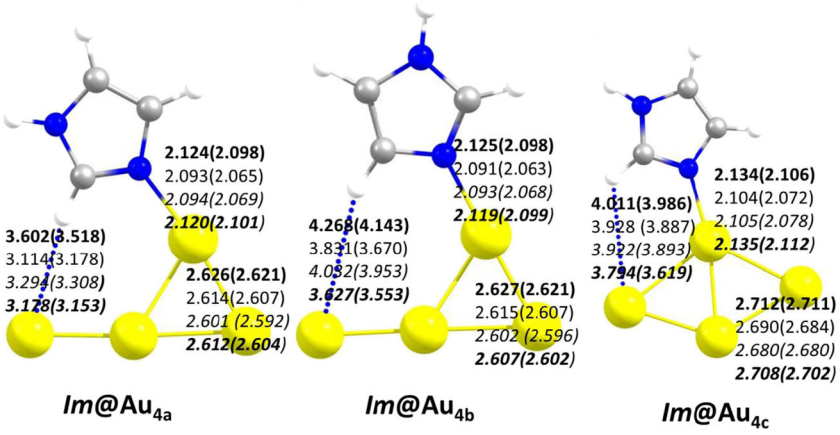

Fig. 2 Optimized geometries of *Im*@Au_4 at B3LYP (*bold*), PBE (*normal*), PBE0 (*italic*) and M05-2X (*bold / italic*) methods using BS1 basis set. Distances in *parenthesis* were computed using BS2. Distances in Ångstroms

than its value in the isolated Au_2 dimer. For CH and NH distances in Im, all electronic structure methods lead to sensitively the same equilibrium distances (Fig. 1). Generally, M05-2X predicts shorter distances than the other DFTs but close to MP2 data and hence predicts stronger interactions between N1···Au in Im@Au_n complexes.

Im@Au₄

For Au_4, a Y-shape, a rhombic and a trans-chain structure are known (see for instance Ref. [5]). For nanoclusters of Au_4 with *Im*, we found three different stable planar conformations: *Im*@Au_{4a}, *Im*@Au_{4b}, and *Im*@Au_{4c} (Fig. 2). *Im*@Au_{4c} is obtained by linking *Im* to rhombic Au_4. *Im*@Au_{4a} and *Im*@Au_{4b} result from attaching *Im* to the Au_4 Y-structure, which is no longer symmetrical due to the unsymmetrical nature of *Im* and, in particular, because of the establishment of the H-bonded interaction (C–H···Au) with the neighboring gold atoms (dashed lines in Fig. 2). Similarly, the more stable symmetrical tetrahedral (T_d) shape of isolated Au_4 within the *Im*@Au_4 cluster converts into *Im*@Au_{4a} during the optimizations (all methods). The creation of this H-bonded interaction may be related to the relatively acidic nature of the C_2-carbon atom in *Im*. Such H-bonds were already noted for the G@Au_2 complex and are known as anchor assisted H-bonds (AAHB) [10]. These H-bonds and weakly bound interactions were confirmed by AIM topography analysis. For illustration, Fig. 7 presents the $\rho(r_c)$ and $\nabla^2\rho(r_c)$ values, with the bond critical points (BCP), the ring critical points (RCP) and the cage critical points (CCP) pointed out. The corresponding NBO analyses and discussions can be found in the ESM.

Similar to *Im*@Au_2, the N1 atom of the *Im* moiety coordinates directly with an Au atom with a computed Au–N1 distance of ~2.1 using either DFT/BS1 or DFT/BS2. The intra *Im* distances are similar to those given in Fig. 1 for *Im*@Au_2. All DFT methods predict Au–Au distances ranging from ~2.6 to 2.7 Å, which are slightly longer than those found for *Im*@Au_2. We compute AAHB distances in the order of 3.6

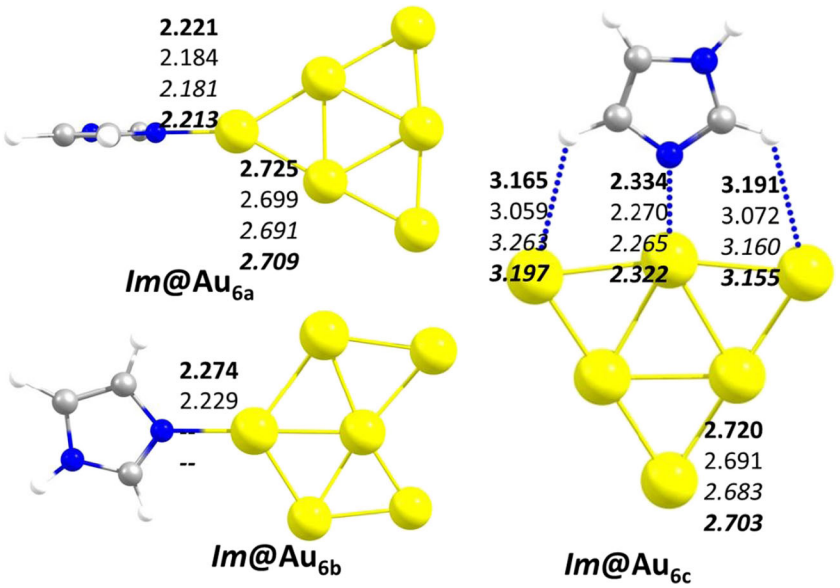

Fig. 3 Optimized geometries of *Im*@Au_6 at B3LYP (*bold*), PBE (*normal*), PBE0 (*italic*) and M05-2X (*bold / italic*) methods using BS1 level. Distances are in Ångstroms

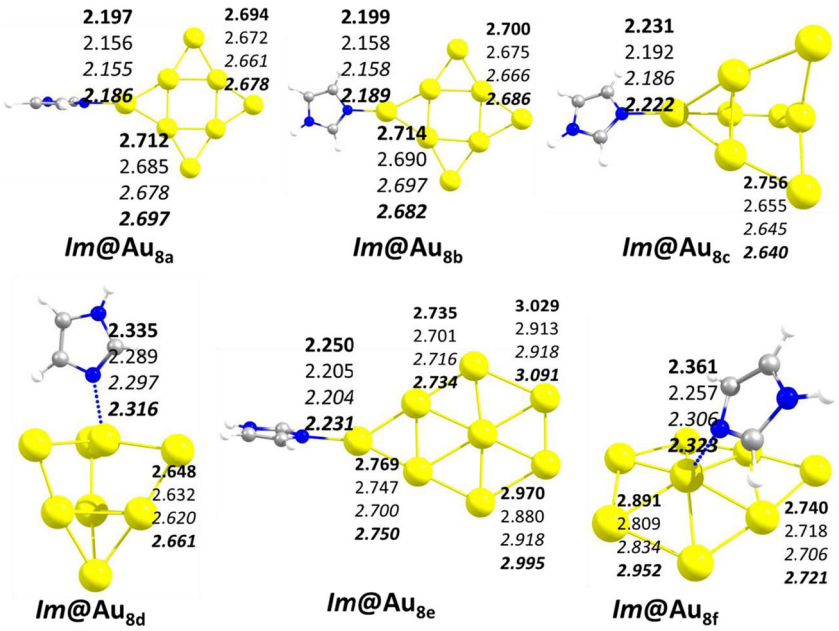

Fig. 4 Optimized geometries of *Im*@Au_8 at B3LYP (*bold*), PBE (*normal*), PBE0 (*italic*) and M05-2X (*bold / italic*) methods using BS1 basis set. Distances are in Ångstroms

and 4.2 Å using B3LYP that reduce by 0.2–0.6 Å using either PBE0 or M05-2X. Figure 2 shows that AAHB distances are distinctly shorter in *Im*@Au_{4a} than in *Im*@$Au_{4b,4c}$. This is in line with the larger BE computed for *Im*@Au_{4a} (Table 1). Generally, the M05-2X functional provides shorter C_2–H Au H-bonds than the other DFTs. M05-2X and PBE0 account for weak interactions at both BS1 and BS2 levels while B3LYP does not. The reliability of these functionals may affect the

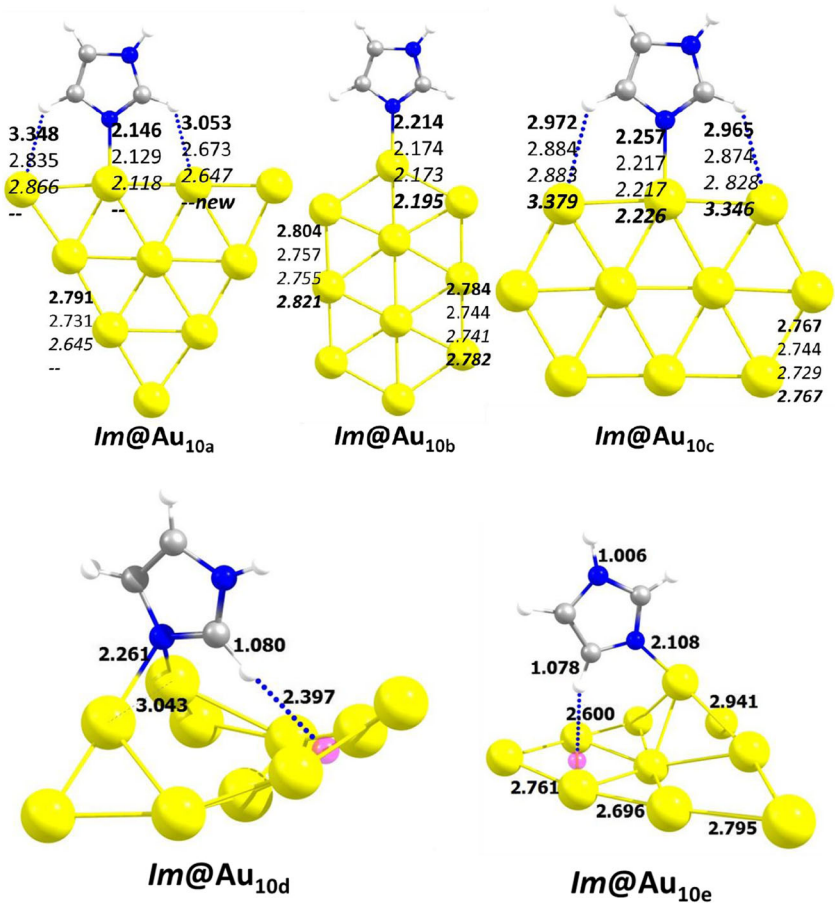

Fig. 5 Optimized geometries of *Im*@Au_{10} at B3LYP (*bold*), PBE (*normal*), PBE0 (*italic*) and M05-2X (*bold / italic*) methods using BS1 basis set. Distances are in Ångstroms

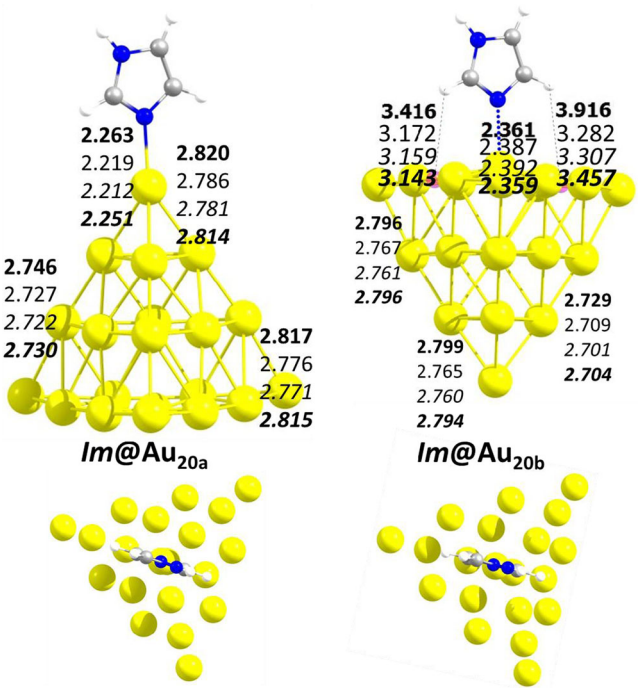

Fig. 6 Optimized geometries of *Im*@Au_{20} at B3LYP (*bold*), PBE (*normal*), PBE0 (*italic*) and M05-2X (*bold / italic*) methods using BS1 basis set. Distances are in Ångstroms. *Upper panel* Front view, *lower panel* top view

energetics of these complexes (see next section). Small changes are observed only in the Au–N1 distance with PBE and PBE0 methods. Moreover, M05-2X and PBE0 always predict shorter NH–Au distances (at AAHB) and hence stronger interactions within both moieties of the *Im*@Au_4 complexes. Moreover, close agreement is found with MP2 results (Table 1). Accordingly, PBE0/BS1 and M05-2X/BS1 levels are suited to the treatment of larger *n* complexes.

Im@Au₆

DFT and ab initio [MP2/CCSD(T)] computations [61] showed that the Au_6 hexamer presents three stable forms of D_{3h}, C_{5v} and D_{4h} symmetries. These were used as starting points to link with *Im*. Figure 3 displays the optimized geometries of *Im*@Au_6 isomers using DFT and BS1. Three isomers were found (*Im*@Au_{6a}, *Im*@Au_{6b} and *Im*@Au_{6c}) where *Im* forms a complex with the Au_6 cluster with an unprotonated nitrogen. *Im*@Au_{6a} consists of a planar Au_6 cluster bonding to *Im*, which is located in the perpendicular plane of the Au_6 plane, whereas both Au_6 and *Im* belong to the same plane in *Im*@Au_{6b} and *Im*@Au_{6c} isomers. Figure S1 in the ESM shows that there is a favorable interaction between the orbitals of N1 and the Au adatom for these configurations. A further charge transfer stabilization through covalent and noncovalent bonds may take place also. Indeed, *Im*@Au_{6a} and *Im*@Au_{6b} present an adatom type of interaction that is characterized by a

Table 1 Calculated basis set superposition error (BSSE)-corrected binding energies (BEs, in kJ mol^{-1}) for *Im*–Au_n (*n*=2 and 4) clusters computed using B3LYP, PBE, PBE0 and M05-2X DFTs with and without inclusion of D3 correction. BEs deduced using MP2 and SCS-MP2 methods are also listed. BS1 and BS2 refer to 6-31+G**ULanl2DZ and aVTZULanl2DZ and the associated basis sets, respectively

Im-Au_n Clusters	B3LYP		PBE		PBE0			M05-2X			MP2@BS2 (SCS-MP2)
	BS1	BS2 (SP) [a]	BS1	BS2 (SP) [a]	BS1	BS2 (SP) [a]	PBE0+D3 [b]	BS1	BS2 (SP) [a]	M05-2X+D3 [b]	
Au_2	−105.4	−136.0 (−113.4)	−126.3	−136.0 (136.0)	−118.9	−128.3 (−128.1)	−135.0	−120.2	−126.2 (−126.1)	−127.2	−155.1 (−136.8)
Au_{4a}	−138.3	−146.3 (−145.7)	−158.4	−167.1 (−167.1)	−154.5	−163.0 (−162.8)	−175.4	−163.2	−168.1 (−168.0)	−170.5	−200.5 (−180.5)
Au_{4b}	−132.9	−141.0 (−140.5)	−151.6	−161.0 (−160.6)	−147.8	−156.7 (−156.4)	−166.9	−155.3	−160.4 (−160.3)	−162.6	−193.0 (−173.4)
Au_{4c}	−122.2	−129.3 (−129.2)	−136.7	−145.6 (−145.1)	−133.9	−142.0 (−141.6)	−153.3	−140.6	−145.2 (−144.1)	−146.5	−181.2 (−160.7)

[a] Values in parenthesis are single point BEs calculated using BS2 basis set. See text for details

[b] Single point BEs including D3 dispersion. See text for details

Table 2 Calculated BSSE corrected binding energies (BEs, in kJ mol^{-1}) of *Im*@Au$_n$ clusters computed using PBE0 and M05-2X and BS1 and BS2 basis sets along with DFT+D3 values

Im@Au$_n$ clusters	PBE0			M05-2X		
	BS1	BS2(SP)	PBE0+D3 [a]	BS1	BS2 (SP)	M05-2X+D3 [a]
Im@Au$_{6a}$	−90.5	−97.6	−106.1	−95.0	−99.5	−101.5
Im@Au$_{6b}$ [b]	–	–	–	–	–	–
Im@Au$_{6c}$	−51.6 [a,c]	−55.7 [a,c]	−72.4[c]	−56.1 [a,c]	−57.5 [a,c]	−60.4[c]
Im@Au$_{8a}$	−102.0	−110.0	−118.8	−106.0	−113.7	−115.9
Im@Au$_{8b}$	−100.0	−108.1	−117.0	−104.5	−111.7	−113.9
Im@Au$_{8c}$	−95.6	−102.5	−112.4	−98.8	−102.8	−105.6
Im@Au$_{8d}$	−43.1[c]	−46.3[c]	−67.7[c]	−59.5[c]	−60.3[c]	−64.6[c]
Im@Au$_{8e}$	−74.7	−81.6	−90.1	−81.1	−85.5	−87.5
Im@Au$_{8f}$	−55.3[c]	−57.7[c]	−84.3[c]	−72.7[c]	−72.9[c]	−78.6[c]
Im@Au$_{10a}$	−134.5	−143.2	−163.3	–	–	–
Im@Au$_{10b}$	−86.4	−93.5	−105.1	−94.8	−98.7	−101.5
Im@Au$_{10c}$	−76.8	−83.2	−102.2	−92.0	−95.2	−98.9
Im@Au$_{10d}$	–	–	–	−223.7[c]	−226.5[c]	−233.2[c]
Im@Au$_{10e}$	–	–	–	−177.8[c]	−182.2[c]	−188.4[c]
Im@Au$_{20a}$	−81.4	−87.8	−98.2	−83.8	−87.6	−90.8
Im@Au$_{20b}$	−28.4[c]	−30.0[c]	−61.5[c]	−52.6[c]	−53.0[c]	−61.3[c]

[a] Single point BEs including D3 dispersion

[b] Converts into *Im*@Au$_{6a}$ at PBE0 and M05-2X methods. See text

[c] BEs of anchor assisted H-bond (AAHB) supported surface models

unique Au–N1 bond, whereas the *Im*@Au$_{6c}$ isomer form is stabilized by three different types of interactions consisting of an Au···N1 bond and two H-bonded (C–H···Au) weak noncovalent interactions as those described above for *Im*@Au$_4$. The Au–N1 distance was computed to be ~2.2 to 2.3 Å. Even though other possible conformations were searched, optimizations led solely to *Im*@Au$_{6a}$, *Im*@Au$_{6b}$ and *Im*@Au$_{6c}$ clusters forms. This is due to orbital overlapping and additional types of noncovalent interactions within these clusters that favor these three conformations. Note that *Im*@Au$_{6b}$ converts into *Im*@Au$_{6a}$ at PBE0/BS1 and M05-2X/BS1 levels.

Im@Au$_8$

The three most stable forms of Au$_8$ are of D_{4h}, C_{2v} and T_d symmetries [62]. When *Im* interacts with Au$_8$, six isomers are found: *Im*@Au$_{8a}$, *Im*@Au$_{8b}$, *Im*@Au$_{8c}$, *Im*@Au$_{8d}$, *Im*@Au$_{8e}$

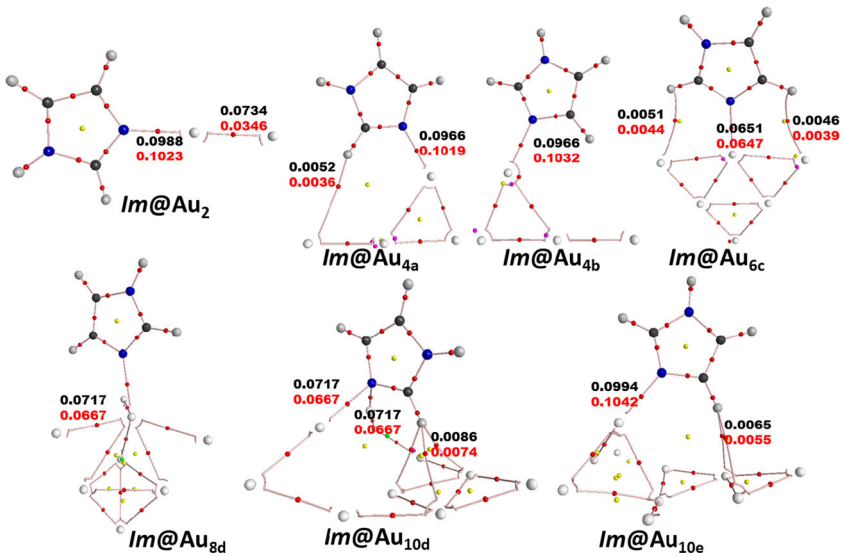

Fig. 7 Molecular graphs of Im@Au$_n$ complexes at M05-2X/BS1 geometries. *Black* $\rho(r_c)$ values, *red* $\nabla^2\rho(r_c)$ values. These values are shown near to the bond paths corresponding to Au···N, C_2–H···Au, and C_5–H···Au interactions. *Red dots* Bond critical points (BCP), *yellow dots* ring critical points (RCP), *green dots* cage critical points (CCP)

and *Im*@Au_{8f} (Fig. 4). In *Im*@$Au_{8a,8b,8e,8f}$, the gold octamer is a planar star-/wheel-like molecule with *Im* either in the gold atom plane or orthogonal to it. In *Im*@Au_{8c} and *Im*@Au_{8d}, *Im* is connected to 3D Au_8 either as an adatom or to the surface of the cluster. For the Au_8 cluster, Hansen et al. [62] recently predicted a similar non-planar structure, which has the lowest energy isomer using CCSD(T). *Im*@Au_{8a}, *Im*@Au_{8b}, *Im*@Au_{8c} and *Im*@Au_{8e} clusters present relatively short Au···N distances (of ~2.2 Å) whereas a slightly longer Au···N distance (of ~2.3 Å) is computed for *Im*@Au_{8d} and *Im*@Au_{8f}. The latter can be considered as models for *Im* adsorbed on an Au(111) surface [63]. It is interesting to discuss the *Im*@Au_{8f} geometry obtained from the M05-2X method. For instance, this cluster shows a structure that is tilted slightly towards gold surface whereas other methods (B3LYP, PBE and PBE0) predict *Im* exactly perpendicular to the surface. Based on our geometrical data, hybrid meta functionals are well suited to the accurate description of covalent and dispersive interactions. No obvious H-bonded interaction (C–H···Au) is visible for *Im*@Au_8. Surprisingly, the PBE method leads to a relatively shorter Au···N distance (2.257 Å) compared to the other DFT methods.

Im@Au₁₀

Optimized geometries of *Im*@Au_{10} complexes are presented in Fig. 5. In total, five structures were computed (*Im*@$Au_{10a–e}$). *Im*@$Au_{10a–c}$ clusters are planar whereas 3D structures were found for *Im*@$Au_{10d–e}$. Interestingly, *Im*@Au_{10} clusters show a transition from 2D to 3D structures as already noted for isolated Au_{10} [64]. For *Im*@$Au_{10a,b,c,e}$ clusters, *Im* links to the Au_{10} cluster via a unique Au–N bond in the N1 atom, whereas the N1 atom of *Im* forms two coordination covalent bonds with two gold atoms with equal distances (of 2.261 Å) in *Im*@Au_{10d}. For *Im*@Au_{10a}, B3LYP, PBE, and PBE0 predict a stable structure, whereas this isomer shows different geometry and converts into *Im*@Au_{10d} using the M05-2X method because of the unequal arrangement of gold atoms at the *Im* interaction site. Here, the excess exchange correlation functional favors geometry reorganization. The other complexes have a double ring (hexagon model) type for gold clusters (i.e., planar) but *Im* forms two different types of interactions. *Im*@Au_{10b} has a unique Au and N1 bond. *Im*@Au_{10e} presents a Au···N bond and an H-bonded interaction (C–H···Au). No H-bonds were found for *Im*@Au_{10a} and *Im*@Au_{10c}. For *Im*@Au_{10d}, a C–H···Au bond was characterized in addition to the two Au···N bonds already noted above, leading to a further stabilization of this isomer. Our results agree with those found for cyclometalated 6-benzylpyridines interacting with gold (III) conformers, where a short Au–N distance ranging from 2.098 to 2.105 Å was predicted using B3LYP/def2-TZVP [65]. In contrast, the calculated Au–N1 bond distances were shorter than in the *Im*@Au(111) surface (i.e., ≈2.3 Å) [63].

Im@Au₂₀

Through analysis of combined photoelectron spectroscopy and density functional results, Li et al. [2] proposed a highly symmetrical tetrahedral structure for Au_{20} gold clusters. Aikens and Schatz [27] suggested two different types of cluster model: (1) a tetrahedral gold cluster similar to that proposed by Li et al. [2] and (2) a vertex model with an adatom structure. The Au_{20} tetrahedral

Binding energies of *Im*@Au_n clusters

In addition to geometries, BEs of complexes are very important in validating suitable DFT methods for the accurate description of noncovalent interactions [45]. The BEs of all complexes were calculated within the supermolecule approach and corrected for basis set superposition error (BSSE) using the procedure suggested by Boys and Bernardi [72]. The counterpoise (CP) method implemented in the Gaussian package was used to carry out BSSE correction. The BEs of various complexes were calculated using the following energy expression:

$$BE = (E_{AB} - (E_A + E_B))$$

where E_{AB} is the total energy of the *Im*@Au_n complex at equilibrium, E_A is the energy of the Au_n gold nanocluster and E_B is the energy of *Im*.

In benchmark computations, we calculated the BEs of *Im*@Au_2 and *Im*@Au_4 using either BS1 or BS2 and DFT approaches. Therefore, their BSSE-corrected BEs calculated at the B3LYP, PBE, PBE0, M05-2X and MP2 (SCS-MP2) methods using BS1 and BS2 [single point (SP)] basis sets are listed in Table 1. BE enhancement was observed when the size of the basis set increases (from BS1 to BS2). Also, using B3LYP, computed BEs at BS1 and BS2(SP) energies were almost equal except for *Im*@Au_2. As expected, the B3LYP/BS1 method was not sufficient to predict the geometry and energies of *Im* and gold clusters. The same BEs at B3LYP and PBE/BS2 levels were in very good agreement with SCS-MP2 rather than MP2 values. Moreover, differences between MP2/BS2 with DFT methods were B3LYP (−19), PBE(−19), PBE0(−27) and M05-2X (−28) (all values are in kJ mol^{-1}). As established in the literature, B3LYP and PBE methods are very suitable for the description of covalent interactions. To scrutinize the ability of these functionals to describe noncovalent types of interaction, we treated *Im*@Au_4 clusters, which are stabilized by both (Au···N and C–H···Au) interactions. M05-2X, PBE and PBE0 methods predict BEs relatively higher than the corresponding B3LYP methods. Values using M05-2X and PBE0 are particularly close to SCS-MP2

values. From this, we conclude that use of PBE and B3LYP methods with BS2 is appropriate for covalently bonded interactions whereas noncovalent interactions need an additional exchange correlation functional (i.e., PBE0 or M05-2X). Finally, SP energies and BEs at optimized structures using either BS1 or BS2 were found to be close. Based on these benchmarks, we calculated the BEs of larger size gold clusters ($n \geq 6$) using the BS2 basis set, where SP computations were performed at the respective optimized structure at the corresponding DFT/BS1 level.

At the M05-2X/BS2 level, we computed BEs of ~ −126, ~ −168, ~ −160 and ~ −145 (in kJ mol^{-1}) for *Im*@Au_2, *Im*@Au_{4a}, *Im*@Au_{4b}, Im@Au_{4c}, respectively. Such large BEs can be explained by the strong Au–N bond created upon complexation. Moreover, isomer *Im*@Au_{4a} is more stable than the other isomers. This is due to the formation of relatively stronger unconventional (C–H···Au) H-bonds between gold and *Im*. *Im*@Au_{4b} possesses an analogous type of interaction but different C–H groups are involved in the AAHB, resulting in a reduction in BE(*Im*@Au_{4b}) reduction by ~8 kJ mol^{-1}. Indeed, it can be found from our calculations that the acidic nature of the C_2–H Au interaction within *Im*@Au_{4a} is relatively stronger than the C_5–H···Au H-bond in *Im*@Au_{4b}.

Table 2 presents the BSSE-corrected BEs computed using PBE0 and M05-2X for *Im*@Au_n (n=6, 8, 10 and 20). The corresponding values computed using B3LYP and PBE are listed in Table S1 of the ESM. Close examination of Table 2 reveals that adatom model isomers are more stable than the other weakly bonded models, except for *Im*@Au_{10} where the 3D isomers (*Im*@Au_{10d} and *Im*@Au_{10e}) exhibit outstanding stability (BEs of ~ −200 kJ mol^{-1}) due to the strong chemical bonds occurring there. These two Au_{10} clusters together with *Im*@Au_{6c}, *Im*@Au_{8d}, *Im*@Au_{8f} and *Im*@Au_{20b} may mimic the Au surface model. The calculated dipole moment value of these clusters is close to zero, hence confirming that these clusters may mimic the surface environment. This is largely corroborated by a smaller Au–N distance (i.e., ≤2.3 Å) for adatom type complexes whereas Au–N distances of ~2.3 Å are computed for surface type models.

At the M05-2X/BS2 level, the calculated BEs for *Im*@Au_{6c}, *Im*@Au_{8d}, *Im*@Au_{8f} and *Im*@Au_{20b} complexes are −57.5, −60.3, −72.9, and −53.0 kJ mol^{-1}, respectively. In particular, Au_8 surface models (Au_{8d} and Au_{8f}) have larger BEs than the other surface mimicking models. This is due to the additional AAHB (C_2–H···Au) interaction within *Im*@Au_{8d} at the bridge site, and to dispersion interactions within the *Im*@Au_{8f} complex. Note that the calculated M05-2X/BS2 BEs (~ −50 kJ mol^{-1}) for surface model clusters are in close agreement with the recent PBE treatment of *Im* adsorbed on a gold (111) surface {*Im*@Au(111), BE=~ −42 kJ/ mol^{-1} [63]} and an earlier PBE study [17] of HIS adsorbed on a gold (111) surface) (HIS@Au(111), BE= −45.6 mol^{-1}).

Tables 1 and 2 also present the D3 corrected PBE0 and M05-2X BEs. For *Im*@Au_2 and *Im*@Au_4, Table 1 shows that an enhancement of BEs is observed for PBE0+D3 (ranging from −7 to–13 kJ mol^{-1}) whereas M05-2X and M05-2X+D3 lead to similar BEs (differences of ~ −2 kJ mol^{-1}). Hence, M05-2X represents better predictions for these complexes than PBE0. These BEs are also in close agreement with the SCS-MP2 method. Similar remarks can be drawn for larger sized gold clusters interacting with *Im* (shown Table 2), where D3 dispersion accounts for −9 to −31 with PBE0 and −2 to −8 kJ mol^{-1} with M05-2X, respectively. The largest deviations are for *Im*@Au_{6c}, *Im*@Au_{8d}, *Im*@Au_{8f} and *Im*@Au_{20b}, which are "surface mimicking models". More generally, our work reveals that dispersions play an important role in the stability of *Im*@Au_n complexes.

AIM analysis

Bader's AIM theory has been employed to quantify the nature of bonding between two molecules or surfaces [53–58]. Several studies have reported characterization of the nature of bonding between organic molecules and metal clusters using AIM parameters [22, 73–76]. AIM can also be used to characterize the agostic type of interaction since it provides more precise quantitative measures with which to describe them. The electron density [$\rho(r_c)$] and Laplacian [$\nabla^2\rho(r_c)$] at the bond critical points (BCPs) of the Au N1, C_2-H Au, and C5-H·Au interactions of molecular graphs are shown in Fig. 7. The red, yellow and green dots indicate BCP, RCP (ring) and CCP (cage), respectively. In addition to $\rho(r_c)$ and its $\nabla^2\rho(r_c)$, other significant parameters such as the kinetic (G_c), potential (V_c), and total (H_c=G_c+V_c) energy density values are provided in Table 3.

The $\nabla^2\rho(r_c)$ values indicate the nature of bonding; in particular, positive and negative values of $\nabla^2\rho(r_c)$ dictate noncovalent and covalent character, respectively [55]. The electronic energy density also provides the valuable information about the nature of bonding. G_c and V_c are always positive and negative, respectively, whereas H_c value depends on the relative magnitude of G_c and V_c. If the G_c value is larger than the absolute value of V_c, the H_c value is positive, thus a purely closed shell interaction is expected. Otherwise, the negative H_c indicates that the interactions correspond to some degree of covalent character. It can be found from our calculated negative values of H_c that all our Au·N1 (Im) complexes are covalent in nature.

Figure 7 shows that the $\rho(r_c)$ values of Im@Au_n clusters range from 0.0608 to 0.0988 a.u. The strongest interaction was found for $Au_{4a,b}$ complexes [$\rho(r_c)$ values of ~0.0966 a.u.) and the interaction at surface models such as Au_{6c}, Au_{8d} and Au_{20b} [$\rho(r_c)$ values range from 0.0608 to 0.0658 a.u.]. $\nabla^2\rho(r_c)$ values exhibited similar trends. The calculated values of $\rho(r_c)$ and $\nabla^2\rho(r_c)$ at the H-bonds (designated as HBCP) for all the

Table 3 Electron density parameters (in a.u.) at Au···N1 in *Im*@Au_n clusters computed at the corresponding M05-2X/BS1 equilibrium geometries. G_c Kinetic energy density, V_c potential energy density, H_c total energy density (=G_c+V_c)

Im@Au_n	$\rho(r_c)$	$\nabla^2\rho(r_c)$	G_c	V_c	H_c
Im@Au_2	0.0988	0.1024	0.0625	−0.0894	−0.0269
Im@Au_{4a}	0.0966	0.1019	0.1245	−0.1472	−0.0226
Im@Au_{4b}	0.0966	0.1032	0.1256	−0.1480	−0.0224
Im@Au_{6c}	0.0651	0.0647	0.0777	−0.0907	−0.0130
Im@Au_{8d}	0.0658	0.0655	0.0787	−0.0920	−0.0133
Im@Au_{10b}	0.0830	0.0869	0.1052	−0.1234	−0.0183
Im@Au_{10c}	0.0782	0.0801	0.0969	−0.1138	−0.0168
Im@Au_{10d}	0.0717	0.0667	0.0829	−0.0990	−0.0161
Im@Au_{10e}	0.0984	0.1042	0.1277	−0.1513	−0.0236
Im@Au_{20b}	0.0608	0.0595	0.0712	−0.0830	−0.0117

clusters ranged from 0.0051 to 0.0092 and 0.0036 to 0.0084 a.u., respectively. These values clearly indicate the involvement of weak H-bonding interactions in the stabilization of these clusters. Close scrutiny of our AIM analysis (see Fig. 7) shows that the C_2–H Au interaction is present only in *Im*@Au_{4a} rather than the Im@Au_{4b} complex (here C5–H···Au) hence rationalizing the observed major stability of *Im*@Au_{4a} vs. Im@Au_{4b}. Similarly, the large BE found for Im@Au_{10d} (~ −233 kJ mol^{-1}) due to the formation of double Au···N1 (Im) bonds (Fig. 5) is also consistent with our $\rho(r_c)$ and $\nabla^2\rho(r_c)$ values at BCPs for this complex. Generally, the calculated electron density at the BCPs correlates roughly with the strength of interaction reported by several authors [77–81].

Vibrational spectroscopy

Table 4 lists the M05-2X/6-31+G** calculated vibrational stretching frequencies, intensities and red/blue shifts. The shifts were calculated from the asymmetric (ν_{as}) and symmetric (ν_{ss}) stretching frequencies of N–H and C–H of isolated *Im*. Upon formation of *Im*@Au_n complexes, the free N–H group in *Im* always red shifts whereas ν_{CH} frequencies are blue-shifted except *Im*@Au_{4a}. Similarly, all free N–H and H-bond N–H have red shifts. It can be observed that the red/blue shifts and intensities of C–H···Au (ν_{C2H}) are significantly higher than that of C–H···Au (ν_{C4H}) interactions. For instance, the calculated ν_{NH}, ν_{C2H} and ν_{C3H} frequency shifts for *Im*@Au_{4a} are −10, −43, and 23 cm^{-1}, respectively. The ν_{NH} shifts range from −50 to −5 $cm^{-1}$and the ν_{C2H} and ν_{C4H} shifts are in the ranges ±43 to 38 cm^{-1} respectively. The largest effect is observed for the *Im*@Au_{4a} complex (−43 cm^{-1}) ν_{C2H} frequency. This is due to the strong AAHB interaction between C_2–H and the gold surface. Moreover, we observed a strong enhancement of the intensity of the N–H stretching bands on the complexes compared to free *Im*. The effects on C–H stretching band intensities were less pronounced. Complexation-induced shifts and changes in the intensity of the corresponding bands can be checked by means of vibrational spectroscopy as performed by Gruene et al. [71] for isolated small gold clusters.

UV–vis spectra

Recent benchmark calculations showed that the PBE0 method is accurate enough for the prediction of the optoelectronic properties [82]. Therefore, UV–vis adsorption spectra of *Im*@Au_n (n = 2–20) complexes along with those of the respective monomers (depicted in Fig. 8) were computed from TDDFT calculations using the PBE0 functional. It can be found from this figure that isolated Au_2 and *Im* exhibit bands below 250 nm, whereas *Im*@Au_n complexes exhibit intense peaks from 400 to 700 nm. It is interesting to note that small-sized clusters with *Im* have bands in both ranges with moderate intensities. Comparison of the spectra in Fig. 8 reveals a significant intensity enhancement as the gold clusters size increases. This is due to the increased efficiency of ligand-to-metal charge transfer in accordance with NBO analysis (cf. ESM)

Systematic changes observed in the absorption spectrum and intensity with cluster size clearly reveals that *Im*@Au_n complexes have potential applications. Recent experimental and theoretical studies on adenine with gold in solution showed similar trends [83]. They also pointed out that, after complex formation, there is an immediate reduction in the intensity of surface plasmon absorbance and a significant red shift in the wavelength (from 525 to 717 nm). Last year, experimental studies on thiol derivatives adsorbed on gold clusters and embedded in polymers [84] showed significant visible fluorescence activity when the thiols were substituted with *Im*, which is in line with the present findings.

General trends

Figure 9 displays the evolution of BEs and Au–N distances versus n for both adatom and surface model clusters at M05-2X/BS2 level. We also give the corresponding values for *Im* adsorbed on Au(111) surface [*Im*@Au(111)] [63]. This figure shows that the calculated |BEs| decrease gradually from Au_2 to the Au_{20}-mer except for *Im*@Au_4 clusters because of the additional unconventional H-bonds (i.e., AAHB) that stabilize such complexes further. For surface model clusters, |BEs| converge smoothly to the corresponding value for *Im*@Au(111). *Im*@Au_8, *Im*@Au_{10} and *Im*@Au_{20} clusters also present some common characteristics with *Im* adsorbed on a Au (111) surface [*Im*@Au(111)]. Therefore, these clusters can be considered as suitable models for investigating

Table 4 Main vibrational stretching frequencies (ν, in cm^{-1}) of isolated *Im* or adsorbed on Au_n (n=2–20) clusters. We give also the band intensities (I, in km mol^{-1}) and the induced shifts (in cm^{-1}) upon complexation. Harmonic vibrational frequencies were computed at the M05-2X/BS1 level of theory and scaled further on by a factor of 0.9445 to derive the corresponding anharmonic frequencies (ν) [86]

Im@Au_n Clusters	Assignment	ν_{calc}	I	Shift	*Im*@Au_n clusters	Assignment	ν_{calc}	I	Shift
Im	ν_{NH}	3,534 3,517[a]	90	–					
	ν_{C2H}	3,113 3,110[a]	1	–					
	ν_{C4H}	3,157 3,143[a]	1	–					
Im@Au_2	ν_{NH}	3,528	151	−7	*Im*@Au_{8d}	ν_{NH}	3,525	162	−9
	ν_{C2H}	3,151	12	38		ν_{C2H}	3,140	6	26
	ν_{C4H}	3,170	1	22		ν_{C4H}	3,159	1	11
Im@Au_{4a}	ν_{NH}	3,524	127	−10	*Im*@Au_{8e}	ν_{NH}	3,527	176	−8
	ν_{C2H}	3,070	70	−43		ν_{C2H}	3,147	15	34
	ν_{C4H}	3,171	1	23		ν_{C4H}	3,166	1	18
Im-Au_{4b}	ν_{NH}	3,529	168	−6	*Im*@Au_{8f}	ν_{NH}	3,528	134	−7
	ν_{C2H}	3,156	9	43		ν_{C2H}	3,127	6	14
	ν_{C4H}	3,170	2	22		ν_{C4H}	3,171	2	23
Im@Au_{4c}	ν_{NH}	3,524	153	−25	*Im*@$Au_{10a/d}$[b]	ν_{NH}	3,484	97	−50
	ν_{C2H}	3,070	10	24		ν_{C2H}	3,113	46	0
	ν_{C4H}	3,171	2	32		ν_{C4H}	3,172	5	24
Im@Au_{6a}	ν_{NH}	3,526	168	−9	*Im*@Au_{10b}	ν_{NH}	3,523	194	−11
	ν_{C2H}	3,146	33	15		ν_{C2H}	3,143	17	30
	ν_{C4H}	3,164	1	16		ν_{C4H}	3,160	2	12
Im@Au_{6c}	ν_{NH}	3,528	146	−7	*Im*@Au_{10c}	ν_{NH}	3,521	189	−13
	ν_{C2H}	3,130	0	17		ν_{C2H}	3,137	11	24
	ν_{C4H}	3,162	1	14		ν_{C4H}	3,157	1	9
Im@Au_{8a}	ν_{NH}	3,526	175	−9	*Im*@Au_{10e}	ν_{NH}	3,525	182	−9
	ν_{C2H}	3,147	15	34		ν_{C2H}	3,139	7	26
	ν_{C4H}	3,165	1	17		ν_{C4H}	3,162	3	14
Im@Au_{8b}	ν_{NH}	3,526	172	−9	*Im*@Au_{20a}	ν_{NH}	3,525	199	−9
	ν_{C2H}	3,147	15	34		ν_{C2H}	3,143	18	30
	ν_{C4H}	3,164	1	16		ν_{C4H}	3,162	1	14
Im@Au_{8c}	ν_{NH}	3,521	178	−13	*Im*@Au_{20b}	ν_{NH}	3,530	158	−5
	ν_{C2H}	31,56	12	43		ν_{C2H}	3,118	8	5
	ν_{C4H}	3,174	1	26		ν_{C4H}	3,155	0.5	7

[a] Experimental values (http://webbook.nist.gov)

[b] Au_{10a} becomes Au_{10d} after optimization at M05-2X method. See text for details

organic molecules interacting with the Au (111) surface at low computational cost. Moreover, the nature of the interaction at AAHB can be quantified from AIM analysis. This clearly reveals that gold can act as a potential H-bond acceptor from different environments. These important findings were confirmed by NBO and AIM analysis (see ESM) and vibrational spectra for these complexes. Recently, Aiswaryalakshmi et al. [74] studied the hydrogen bonded complexes formed between the square pyramidal $Fe(CO)_5$ with HX (X=F, Cl, Br). They showed that Fe can act as a strong H-bond and halogen bond acceptor [74]. Similarly, Sun and Felice [22] found that gold can act as H-bond acceptor with biomolecules (N–H···Au and N/O···Au). In addition, very recent investigations on Au_n clusters with halogen molecules revealed the covalent nature of the interaction between gold and halogen(s) within such clusters [75], whereas further stabilization is ensured by the occurrence of noncovalent interactions between gold and their complexes as in the present case.

Both BEs and structures of *Im*@Au_n clusters clearly show that various types of noncovalent interaction stabilize these complexes. AIM analysis indicates the involvement of weak H-bonding interactions in the stabilization

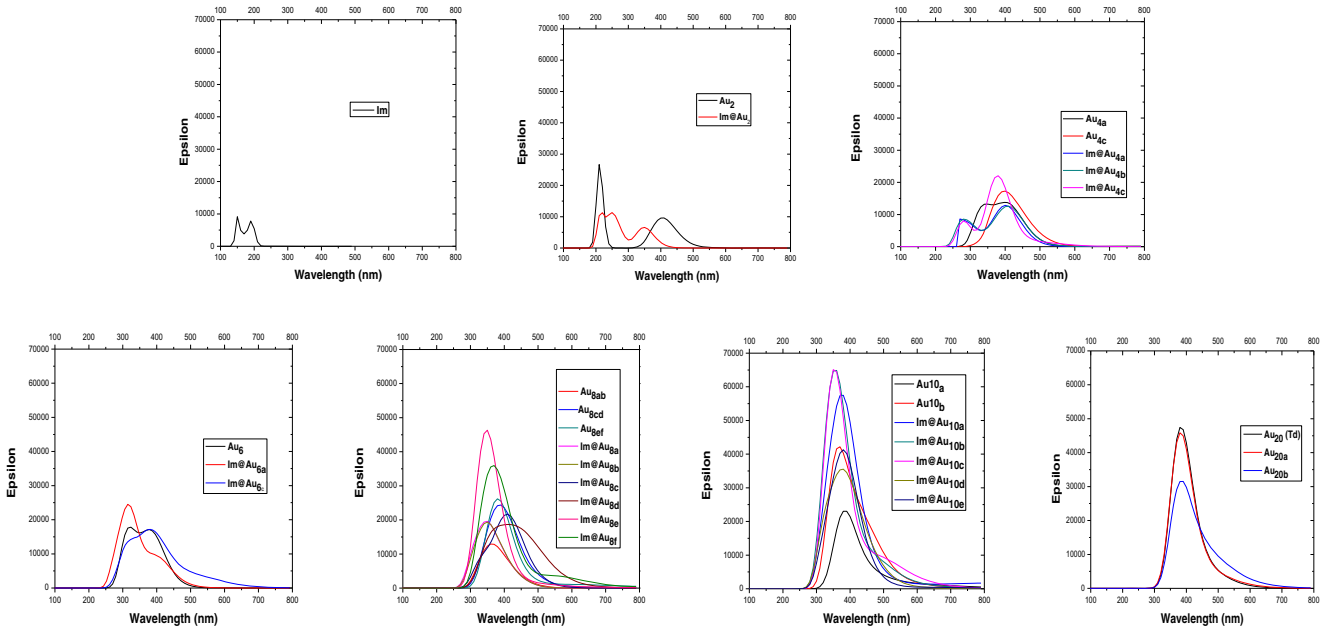

Fig. 8 UV-vis spectra of *Im*, isolated Au_n clusters and *Im*@Au_n complexes

of these clusters in addition to the Au–N bond for which a donor-acceptor type interaction was confirmed by NBO analysis (see ESM for further details). Indeed, the donor-acceptor interactions in these clusters involve the interaction of the lone pairs of the N1 nitrogen atom [LP(1)N1] of *Im* and Au clusters antibonding orbitals (cf. Table S2). For *Im*@Au_2, the charge transfer from lone pair of N1 to the antibonding orbital of gold [BD*(1)Au–Au] is higher than the LP(1)N to LP*(1)Au interactions. Therefore, the nature of N1 and the Au1 bond is covalent. Similarly, charge transfer in *Im*@Au_{6c} and *Im*@Au_{20b} (surface models) exhibits such LP(1)N to LP*(1) Au interactions. An analogous type of charge transfer interaction is also observed in adatom models (*Im*@ Au_{6a}, Au_{8a}, Au_{8b}, Au_{10a} and Au_{20a}). Back bonding effects of gold to *Im* and intra molecular charge transfer in *Im* play crucial roles in *Im*@Au_n complexes. Especially, significant space through charge transfer from the LP of gold [LP*(6)Au1) to C2 and C5 atoms of *Im* (RY*(2)C2(5)] was observed from our surface model (*Im*@Au_{20b}). In addition, charge transfer characterization features of these complexes have also been observed from their shape in frontier molecular orbital analysis. For illustration, Figures S1 and S2 display the isosurface density (0.02 a.u) plots for the *Im*@Au_n complex calculated at PBE0/BS1. Both surface models *Im*@Au_{6c}, and *Im*@Au_{20b} complex HOMO

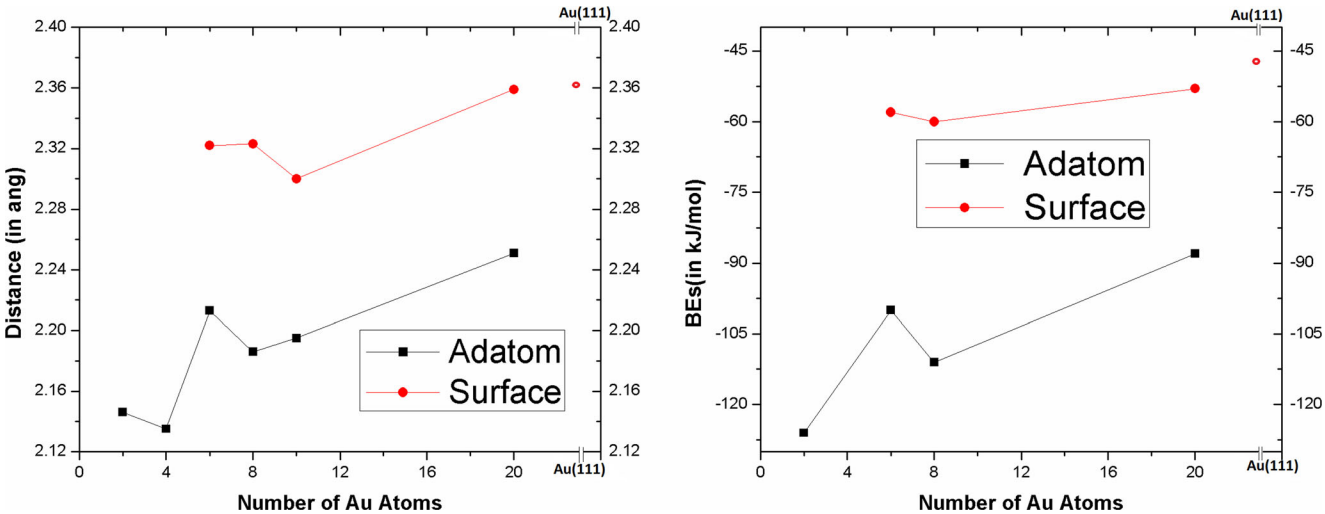

Fig. 9 Evolution of the Au–N distances and BEs of *Im*@Au_n complexes vs *n* at M05-2X/BS2 level compared with the Im@Au(111) surface [63]

orbitals are localized on the N atom of *Im* and the corresponding LUMO orbitals are localized mostly at gold clusters.

Conclusions

We treated *Im*@Au_n (n=2, 4, 6, 8, 10, and 20) complexes using various DFT functionals and basis sets. We found that electron correlation plays a crucial role in the description of these organo-metal complexes and at interfaces. Our work establishes the capability of GGA-PBE0 and M05-2X functionals for providing accurate results for the chemisorption of small molecules on metal clusters and for physisorption, which is dominated mostly by vdWs interactions.

Upon complexation of *Im* with Au_n clusters, strong Au···N bonds occur between Au and the deprotonated nitrogen of *Im* as well as weak C–H···Au H-bond interactions [unconventional type of AAHB (C_2–H···Au)]. Vibrational, AIM and NBO analyses revealed the role of various types of noncovalent interactions in the stability of these complexes. On the whole, *Im* molecular arrangements at gold clusters depend on both covalent and dispersive interactions. Principally, surface mimicking models (such as *Im*@Au_{6c}, *Im*@Au_{8d}, *Im*@Au_{8f} and *Im*@Au_{20b}) have more of a dominant dispersion effect than the other, adatom-type, complexes. Finally, we characterized a strong bond between *Im* and Au_n species that may serve for self-assembled monolayers (SAMs) of organic molecules on gold instead of the well-known gold–sulfur ones for further applications of SAMs [85].

Acknowledgments The authors would like to extend their sincere appreciation to the Deanship of Scientific Research at King Saud University for funding the research through the Research Group project No. RGP-VPP-333. We are also grateful for a Marie Curie International Research Staff Exchange Scheme Fellowship within the 7th European Community Framework Programme under Grant No. IRSES-GA-2012-31754, the COST Action CM1405 MOLIM. M.P. thanks LABEX Modélisation & Expérimentation pour la Construction Durable (MMCD, U. Paris-Est) for financial support and Prof. V. Subramanian (CSIR-CLRI, Chennai, India) for fruitful discussions.

References

1. Boyen HG, Kastle G, Weigl F, Koslowski B, Dietrich C, Ziemann P, Spatz JP, Riethmuller S, Hartmann C, Moller M, Schmid G, Garnier MG, Oelhafen P (2002) Science 297:1533–1536
2. Li J, Li X, Zhai HJ, Wang LS (2003) Science 299:864–867
3. Pyykko P (2004) Angew Chem Int Ed 43:4412–4456
4. Pyykko P (2008) Chem Soc Rev 37:1967–1997
5. Hakkinen H (2008) Chem Soc Rev 37:1847–1859
6. Yang Z, Leon I, Wang LS (2013) J Chem Phys 139:021106
7. Wang J (2000) Nucleic Acids Res 28:3011–3016
8. Lynch I, Salvati A, Dawson KA (2009) Nat Nano 4:546–547
9. Sindhu K, Rajaram A, Sreeram KJ, Rajaram R (2014) RSC Adv 4: 1808–1818
10. Zhang L, Ren T, Yang X, Zhou L, Li X (2013) Int J Quantum Chem 113:2234–2242
11. Zhang X, Sun CQ, Hirao H (2013) Phys Chem Chem Phys 15: 19284–19292
12. Kryachko ES, Remacle F (2005) J Phys Chem B 109:22746–22757
13. Rosa M, Corni S, Felice RD (2012) J Phys Chem C112:21366–21373
14. Kumar A, Mishra PC, Suhai S (2006) J Phys Chem A 110:7719–7727
15. Lv G, Wei F, Jiang H, Zhou Y, Wang X (2009) J Mol Struct (THEOCHEM) 915:98–104
16. Martinez A (2010) J Phys Chem C 114:21240–21246
17. Iori F, Corni S, Felice RD (2008) J Phys Chem C 112:13540–13545
18. Cossaro A, DellAngela M, Verdini A, Puppin M, Kladnik G, Coreno M, Simone M, Kivimaki A, Cvetko D, Canepa M, Floreano L (2010) J Phys Chem C 114:5011–15014
19. Storhoff JJ, Elghanian R, Mirkin CA, Letsinger RL (2002) Langmuir 18:6666–6670
20. Martinez A (2009) J Phys Chem A 113:1134–1140
21. Shukla MK, Dubey M, Zakar E, Leszczynski J (2009) J Phys Chem C 113:3960–3966
22. Sun W, Felice RD (2012) J Phys Chem C 116:24954–24961
23. Jena NK, Chandrakumar KRS, Ghosh SK (2012) J Phys Chem C 116:17063–17069
24. Tao NJ, de Rose JA, Lindsay SM (1993) J Phys Chem 97:910–919
25. Jalkanen J, Zerbetto F (2006) J Phys Chem B 110:5595–5601
26. Ihm H, Ajo H, Gottfried J, Bera P, Campbell C (2004) J Phys Chem B 108:14627–14633
27. Aikens CM, Schatz GC (2006) J Phys Chem A 110:13317–13324
28. Cao GJ, Xu HG, Li RZ, Zheng W (2012) J Chem Phys 136:014305
29. Kladnik G, Cvetko D, Batra A, Dell'Angela M, Cossaro A, Kamenetska M, Venkataraman L, Morgante A (2013) J Phys Chem C 117:16477–16482
30. Pasteka L, Rajsky T, Urban M (2013) J Phys Chem A 117:4472–4485
31. Dunning TH Jr (1989) J Chem Phys 90:1007–1023
32. Dupuis M, Rys J, King HF (1976) J Chem Phys 65:111–116
33. Kendall RA, Dunning TH, Harrison RJ (1992) J Chem Phys 96: 6796–6806
34. Hay PJ, Wadt WR (1985) J Chem Phys 82:299–310
35. Frisch MJ et al. (2009) Gaussian 09 Revision, A. 1, Gaussian Inc, Wallingford, CT
36. Furche F, Ahlrichs R, Weis P, Jacob C, Gilb S, Bierweiler T, Kappes MM (2002) J Chem Phys 117:6982
37. Xiao L, Tollberg B, Hu X, Wang L (2006) J Chem Phys 124:114309
38. Assadollahzadeh B, Schwerdtfeger P (2009) J Chem Phys 131: 064306
39. David J, Guerra D, Restrepo A (2009) Chem Phys Lett 539:64–69
40. Staroverov VN, Scuseria GE, Tao J, Perdew JP (2003) J Chem Phys 119:12129
41. Grimme S (2004) J Comput Chem 25:1463–1473
42. Zhao Y, Truhlar DG (2005) Phys Chem Chem Phys 7:2701–2705
43. Zhao Y, Lynch BJ, Truhlar DG (2005) Phys Chem Chem Phys 7:43–52
44. Schultz NE, Zhao Y, Truhlar DG (2005) J Phys Chem A 109:4388–4403
45. Prakash M, Gopalsamy K, Subramanian V (2011) J Chem Phys 135: 214308
46. Curtiss LA, Redfern PC, Raghavachari K, Rassolov V, Pople JA (1999) J Chem Phys 110:4703
47. Grimme S (2003) J Chem Phys 118:9095
48. Werner HJ et al. (2012) Molpro 2012.1 a package of ab initio programs (http://www.molpro.net.)
49. Bachorz RA, Bischoff FA, Hofener S, Klopper W, Ottiger P, Leist R, Frey JA, Leutwyler S (2008) Phys Chem Chem Phys 10:2758–2766

50. Grimme S (2006) J Comput Chem 27:1787–1799
51. Grimme S (2006) J Chem Phys 124:034108
52. Grimme S, Antony J, Ehrlich S, Krieg H (2010) J Chem Phys 132: 154104
53. Biegler-Konig F, Schonbohm J, Derdau R, Bayles D, Bader RFW (2000) AIM version 1; Bielefeld, Germany
54. Bader RFW (1990) Atoms in molecules. a quantum theory. Oxford University Press, New York
55. Grabowski SJ, Sokalski WA, Dyguda E, Leszczynski J (2006) J Phys Chem B 110:6444–6446
56. Parthasarathi R, Subramanian V, Sathyamurthy N (2007) J Phys Chem A 111:13287–13290
57. Prakash M, Gopalsamy K, Subramanian V (2009) J Phys Chem A 113:13845–13852
58. Kumar RM, Elango M, Subramanian V (2010) J Phys Chem A 114: 4313–4324
59. Prakash M, Subramanian V (2011) Phys Chem Chem Phys 13: 21479–21486
60. Glendening ED, Reed AE, Carpenter JA, Weinhold F, NBO Version 31
61. Han Y-K (2006) J Chem Phys 124:024316
62. Hansen JA, Piecuch P, Levine BG (2013) J Chem Phys 139:091101
63. Prakash M, Mathivon K, Benoit DM, Chambaud G, Hochlaf M (2014) Phys Chem Chem Phys 16:12503–12509
64. Götz DA, Schäfer R, Schwerdtfeger P (2013) J Comp Chem 34: 1975–1981
65. Schmidbaur KFH, Al-juaid SS (2013) Inorg Chem 19:9669–9674
66. Zhao HY, Ning H, Wang J, Su XJ, Guo XG, Liu Y (2010) Phys Letters A 374:1033
67. Ford MJ, Soulé de Bas B, Cortie MB (2007) Mat Sci Eng B 140:177
68. Kryachko ES, Remacle F (2007) Int J Quant Chem 107:2922–2934
69. Zhao LX, Lei YM, Zhang M, Feng XJ, Luo YH (2009) Physica B 404:1705
70. Yang A, Fa W, Dong J (2010) Phys Lett A 374:4506
71. Gruene P, Rayner DM, Redlich B, van der Meer AFG, Lyon JT, Meijer G, Fielicke A (2008) Science 321:674–676
72. Boys SF, Bernardi F (1970) Mol Phys 19:553–566
73. Jamshidi Z, Farhangian H, Tehrani AZ (2013) Int J Quan Chem 113: 1062–1070
74. Aiswaryalakshmi P, Mani D, Arunan E (2013) Inorg Chem 52:9153–9161
75. Zhao Q (2014) J Mol Model 20:2133–2138
76. Shankar R, Kolandaivel P, Senthilkumar L (2010) J Phys Org Chem 24:553–567
77. Scheiner S, Grabowski SJ, Kar T (2001) J Phys Chem A 105:10607–10612
78. Grabowski SJ (2001) J Phys Chem A 105:10739–10746
79. Parthasarathi R, Subramanian V, Sathyamurthy N (2006) J Phys Chem A 110:3349–3351
80. Parthasarathi R, Raman SS, Subramanian V, Ramasami T (2007) J Phys Chem A 111:7141–7148
81. Mandal A, Prakash M, Kumar RM, Parthasarathi R, Subramanian V (2010) J Phys Chem A 114:2250–2258
82. Solomon RV, Bella AP, Vedha SA, Venuvanalingam P (2012) Phys Chem Chem Phys 14:14229–14547
83. Arikrishnan J, Sheerin SKT, Murugavelu M, Karthikeyan B (2011) Indian J Chem 50A:46–50
84. Carotenuto G, Nicola D, Nicolais L (2013) Adv Mater Sci Eng 54: 8284
85. Häkkinen H (2012) Nat Chem 4:443–455
86. Merrick JP, Moran D, Radom L (2007) J Phys Chem A 111:11683–11700